CrossMark

ORIGINAL PAPER

A subaqueous hazard map for earthquake-triggered landslides in Lake Zurich, Switzerland

M. Strupler[1,2] · L. Danciu[2] · M. Hilbe[3] · K. Kremer[2] ·
F. S. Anselmetti[3] · M. Strasser[1,4] · S. Wiemer[2]

Abstract The awareness of geohazards in the subaqueous environment has steadily increased in the past years and there is an increased need to assess these hazards in a quantitative sense. Prime examples are subaqueous landslides, which can be triggered by a number of processes including earthquakes or human activities, and which may impact offshore and onshore infrastructure and communities. In the literature, a plenitude of subaqueous landslide events are related to historical earthquakes, including cases from lakes in Switzerland. Here, we present an approach for a basin-wide earthquake-triggered subaquatic landslide hazard assessment for Lake Zurich, which is surrounded by a densely populated shoreline. Our analysis is based on high-resolution sediment-mechanical and geophysical input data. Slope stabilities are calculated with a grid-based limit equilibrium model on an infinite slope, which uses Monte Carlo sampled input data from a sediment-mechanical stratigraphy of the lateral slopes. Combined with probabilistic ground-shaking forecasts from a recent national seismic hazard analysis, subaquatic earthquake-triggered landslide hazard maps are constructed for different mean return periods, ranging from 475 to 9975 years. Our results provide a first quantitative landslide hazard estimation for the lateral slopes in Lake Zurich. Furthermore, a back-analysis of a case-study site indicates that pseudostatic accelerations in the range between 0.04 and 0.08 g were needed to trigger a well-investigated subaqueous landslide, dated to ~ 2210 cal. years B.P.

✉ M. Strupler
   michael.strupler@erdw.ethz.ch

1   Geological Institute, ETH Zurich, Sonneggstrasse 5, 8092 Zurich, Switzerland

2   Swiss Seismological Service, ETH Zurich, Zurich, Switzerland

3   Institute of Geological Sciences and Oeschger Centre for Climate Change Research, University of Bern, Bern, Switzerland

4   Institute of Geology, University of Innsbruck, Innsbruck, Austria

1 Introduction

A geohazard can be described as the "probability that a geological state, which creates a particular threat to humans, property and their environment, occurs within a given period of time" (ISSMGE 2004; Hoffmann and Reicherter 2016). Geohazards are therefore mostly characterized by their intensity and recurrence rate (Bollinger 1996). In the sub-aqueous environment, the assessment of hazards has become more important in recent years (e.g. Lee and Jones 2014; Mueller et al. 2016). Such hazards include subaqueous landslides and tsunamis, which may cause damage to infrastructure and loss of lives (e.g. Hoffmann and Reicherter 2016; Lee and Jones 2014). Subaqueous landslides can be triggered by various processes, such as earthquakes, wave loading or human activity. Apart from a trigger mechanism, a favourable topography and the necessary amount of sediments need to be present for a subaqueous landslide to occur (Nadim et al. 1996).

Landslide hazard maps provide the database required to reduce damage, costs and other consequences of landsliding (Aleotti and Chowdhury 1999). For the construction of landslide hazard maps, the failure susceptibility of a slope and the probability of a specific trigger need to be assessed (e.g. Wang et al. 2005).

Sublacustrine landslides have been documented worldwide, and many of them were interpreted as earthquake-triggered (Chapron et al. 1999; e.g. Moernaut et al. 2007; Moernaut and De Batist 2011; Waldmann et al. 2011; Smith et al. 2013; Praet et al. 2016). In Switzerland, subaqueous landslides are common features in perialpine lakes. Also here, a plenitude of subaqueous landslide events have been related to past earthquakes, with various consequences (Schnellmann et al. 2002; Monecke et al. 2004; Strasser and Anselmetti 2008; Strasser et al. 2013; Kremer et al. 2015; Reusch et al. 2016). Evidence of tsunamis triggered by landslides has been documented for Lakes Lucerne (central Switzerland) and Lake Geneva (southwestern Switzerland) (Schnellmann et al. 2002; Kremer et al. 2012; Hilbe and Anselmetti 2015). The tectonics of Switzerland are strongly affected by the Alpine orogeny. In terms of overall crustal strain rate and seismicity rate, Switzerland is located in the transition zones between areas of high seismic activity (Greece, Italy) and areas of low seismic activity (Northern Europe). Damaging earthquakes occur on a regular basis and earthquakes are in fact the natural hazard with the highest risk potential (Wiemer et al. 2009). A well-established historical and paleoseismic catalogue of earthquakes exists (Fäh et al. 2011; Wiemer et al. 2009).

For Lake Zurich, a perialpine Lake in northern Switzerland, Strasser and Anselmetti (2008) identified and mapped a total of 149 landslide deposits in the postglacial sedimentary basin infill (past ∼17,000 years) using reflection seismic data. The authors evaluated five landslide events as earthquake-triggered, as multiple mass-movement deposits occur simultaneously. A high-resolution bathymetric dataset of Lake Zurich (Strupler et al. 2015) allowed the identification, mapping and characterization of features related to landslides that occurred during the past ∼5000 years. Apart from the landslides interpreted as earthquake triggered, a few subaquatic landslides with headscarps in shallow water depths (i.e. <10 m) have occurred in the past 150 years, triggered by onshore human activity (Heim 1876; Kuen 1999). Similar shore collapses leading to landslides have also been documented for the marine environment (e.g. Dan et al. 2007; L'Heureux et al. 2013). Today, ∼247,000 people are living within 1 km distance from the shoreline of Lake

Zurich (Henriod et al. 2016). The regular occurrence of subaqueous landslides in Swiss perialpine lakes, triggered by different mechanisms, emphasizes the need for the assessment of the subaquatic landslide hazard. In this study we focus on the earthquake-triggered landslide hazard, as earthquakes represent the most common cause for large and multiple slide events on the slopes.

Strupler et al. (2017) constructed a sediment-mechanical stratigraphy of Lake Zurich's postglacial lateral slopes. This sediment-mechanical slope characteristics were used to assess the stability at a case-study site with a limit equilibrium approach on an infinite slope for selected locations. The main objectives of this study are to develop a methodology for the mapping of the earthquake-triggered, subaqueous landslide hazard, and to test it on Lake Zurich (Switzerland).

In particular, the following steps are performed and the respective research questions are answered:

Basin-wide modelling of sediment thicknesses

- How much potentially mobile sediment is available in which region of the lateral slopes?

Back-analysis of paleoseismic shaking

- What are the ranges of the back-calculated earthquake accelerations that were required to create the slope failures during known events?
- What limits the spatial extent of the pre-existing landslide features?

Basin-wide landslide susceptibility for the present-day situation

- Which lateral slopes in the basin are susceptible to failure for a static case (i.e. because of high sediment loading and without an external trigger)?

Subaqueous earthquake-induced landslide hazard map

- What is the earthquake-induced landslide hazard for different ground acceleration exceedance probabilities?

2 Setting of the study area and previous studies

2.1 Study site: central basin of Lake Zurich, Switzerland

This study concentrates on the lateral slopes of the up to 136 m deep, central basin of Lake Zurich (Switzerland), as this is the region where most documented subaqueous landslides occurred (Nipkow 1927; Kelts 1978; Strasser et al. 2013). The major geomorphic characteristics (Fig. 1) are a flat basin plain and the relatively steep lateral slopes containing deltas, landslide features and gullies. Six relatively small deltas (cross-hatched in Fig. 1c) are formed by local creeks. Geomorphic expressions of subaqueous landslides can be identified on both lateral (i.e. NE and SW oriented) slopes. The landslide extents show translation areas (dashed areas) and deposition lobes expressing sediment removal, mobilization and deposition. The observed gullies (i.e. small channels that are often parallel to one another and to the local slope gradient, with consistent width and spacing; Field et al. 1999) are located on the steepest slopes (i.e. >25° slope gradient) and originate at the transition from the shallow shore platform to the steep slope. Because of a lack of understanding the processes leading to delta failures (e.g. Hilbe and Anselmetti 2014), we
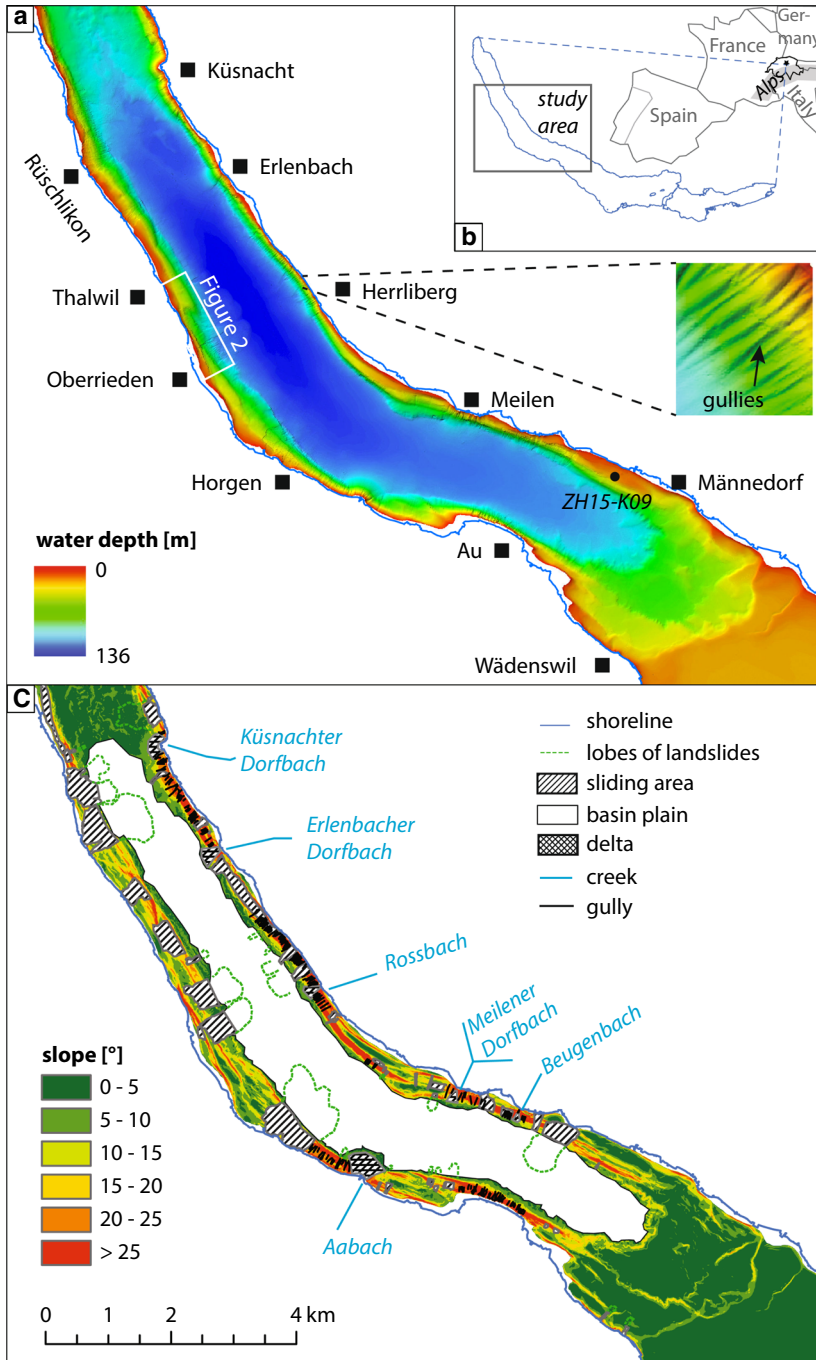
Fig. 1 **a** Digital depth model (DDM) of Lake Zurich's deep basin as shaded relief with colour-coded water depth. Data: Strupler et al. (2015). **b** Location of the study area in Lake Zurich in the greater context. **c** Slope gradient representation with mapped geomorphic features

only consider non-deltaic lateral slopes in the following earthquake-triggered landslide assessment. Also, zones, where the translation areas of past failures are still identifiable in the DDM (Strupler et al. 2015) are excluded from the calculations.

Various datasets available from previous work form the basis of the current study: We consider the landslide catalogue by Strasser and Anselmetti (2008), which was later included in a paleoseismic event catalogue for Central Switzerland (Strasser et al. 2013), outcomes of the probabilistic seismic hazard model of Switzerland (Wiemer et al. 2016), a bathymetric dataset and landslide extents from Strupler et al. (2015), and a mechanical stratigraphy of the postglacial sediment covering the lateral slopes of Lake Zurich (Strupler et al. 2017). The present-day lateral slopes of Lake Zurich show various prehistoric and historical slides, each with a different surface roughness of the translation area (Fig. 2), according to their ages (see Strupler et al. 2015).

2.2 Late Quaternary earthquakes

As the historical seismic record of Switzerland spans only $\sim$1000 years (Fäh et al. 2011), the inclusion of paleoseismological information from lake sediments is an important tool for extending the knowledge on the occurrence of earthquakes (e.g. Strasser et al. 2006, 2013). Paleoseismic records indicate that the foreland region of Zurich may have experienced every few thousand years strong seismic events [with intensity (I) $\geq$ VII] that triggered basin-wide slope stabilities (Strasser et al. 2006). From the five assumedly earthquake-triggered events in Lake Zurich, Strasser et al. (2013) categorized three as 'major events' ($\sim$2210, $\sim$11,600 and $\sim$13,760 cal. years B.P.), which assumedly caused also slope instabilities in Lake Lucerne at a distance of $\sim$40 km. The effect of earthquake shaking on lacustrine sediments has been quantified for Lake Lucerne by calculating a minimal critical pseudostatic acceleration of 0.034 g (Strasser et al. 2007, 2011) to cause the slope to fail for a prehistoric earthquake ($\sim$2220 cal. years B.P.).
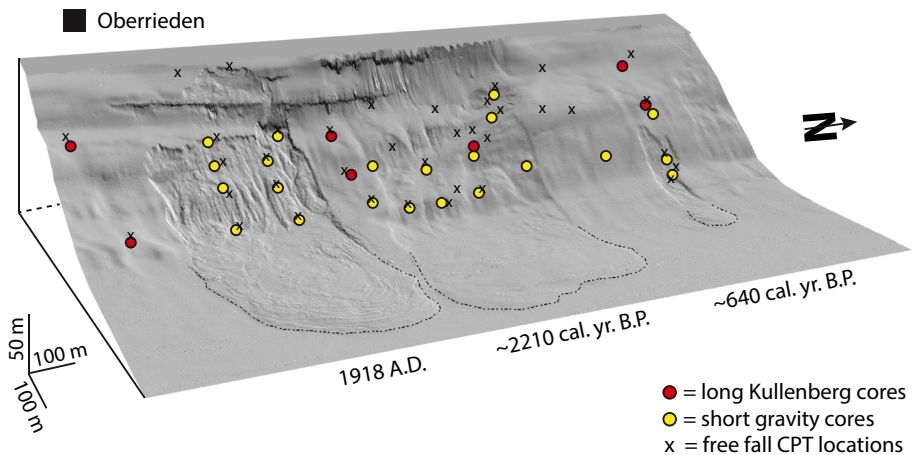

Fig. 2 Subaqueous landslides offshore the village of Oberrieden (location on Fig. 1) with the positions of the retrieved sediment cores and CPT-sites. View towards Northwest. Modified from Strupler et al. (2017)

2.3 Sediment-mechanical stratigraphy on the postglacial, lateral slopes of Lake Zurich

The mechanical stratigraphy of the postglacial sediments on the lateral slopes of Lake Zurich (Strupler et al. 2017) is based on data from six up to 6 m long Kullenberg-type (Kelts et al. 1986) sediment cores and corresponding free fall CPT (Cone Penetrometer Testing) profiles that were taken on the case-study site offshore Oberrieden (Figs. 1a, 2). The Oberrieden site was used for the design of the conceptual model, since it shows three well-constrained subaqueous landslides with known ages that were assigned to different triggers (Strasser and Anselmetti 2008). Four sediment-mechanical units (SMU) were defined based on characteristic patterns of the bulk density (ρ_{bulk}) and undrained shear strength (s_u) (Table 1; Fig. 3a; Strupler et al. 2017). The lowermost unit SMU1 shows typical ρ_{bulk}-values of >1600 kg/m^3 and s_u values that increase from $\sim$5000 Pa at the unit top to $\sim$10,000 Pa at the unit base. In SMU2, ρ_{bulk} decreases from $\sim$1500 to 1350 kg/m^3 and the s_u values fluctuate strongly. SMU3 is defined by a convex shape in the ρ_{bulk} profile, increasing with depth from values of $\sim$1350 to $\sim$1500 kg/m^3 and by constant s_u values of $\sim$5000 Pa. The topmost sediment-mechanical unit shows linearly increasing profiles with depth of ρ_{bulk} and s_u (from $\sim$1300 to $\sim$1350 kg/m^3 and from $\sim$1000 to $\sim$4000 Pa, respectively).

The fact that SMU2 has relatively high s_u values despite its low bulk density has also been observed with laboratory measurements. This may be related to organic material found in that unit, which may keep the sediment together. However, the spatial variability in SMU2 is also relatively large (Strupler et al. 2017).

The thicknesses of the sediment-mechanical units were derived based on information from core to seismic correlation, for locations with available reflection seismic data. The mechanical profiles per unit, including the spatial variability, were then adapted to local thicknesses of each mechanical unit.

The spatial variability of the mechanical data from the input cores allowed to create log-normal distributions of the ρ_{bulk} and s_u for each depth step. To incorporate uncertainty due to the spatial variability of the ρ_{bulk} and s_u values, a Monte Carlo simulation (MCS) was carried out. Hereby, random values from the distributions were subsequently picked for each depth step. 1D-slope stabilities were then calculated probabilistically and deterministically (Fig. 3b): Probability of failure (PoF) versus depth profiles were calculated for selected locations with a limit equilibrium slope-stability assessment (SSA) on an infinite slope. The deterministic factor of safety (FS) was calculated by using the mean of the sediment-mechanical input data per depth step (for details see Strupler et al. 2017). The modelled data, as well as groundtruth data from short sediment cores (Fig. 2), showed that

Table 1 Postglacial lithologic units, their ages and corresponding sediment-mechanical units (Strasser and Anselmetti 2008; Strupler et al. 2017)

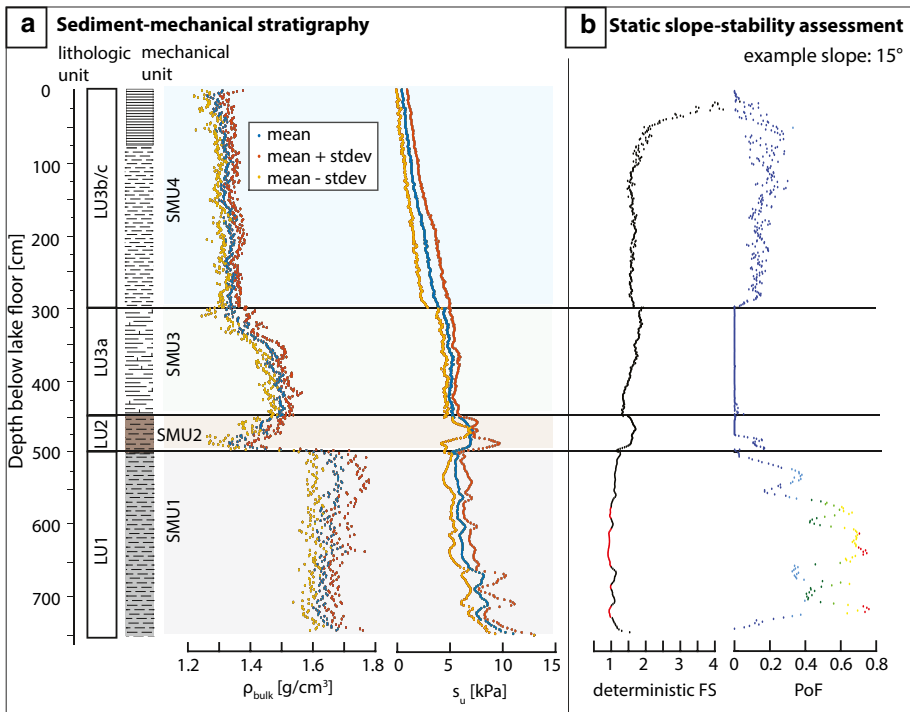| Lithologic unit (LU)	Corresponding sediment-mechanical unit (SMU)
LU3b/c: lacustrine marls: present day to $\sim$7000 cal. years B.P.	SMU4
LU3a: lacustrine chalks: $\sim$7000 to $\sim$12,000 cal. years B.P.	SMU3
LU2: iron sulphide muds: $\sim$12,000 to $\sim$14,500 cal. years B.P.	SMU2
LU1: Late Glacial plastic muds: $\sim$14,500 to $\sim$17,600 cal. years B.P.	SMU1

Fig. 3 **a** Sediment-mechanical stratigraphy, showing characteristic patterns of the bulk density (ρ_{bulk}) and undrained shear strength (s_u) per mechanical unit. Modified from Strupler et al. (2017). **b** Deterministic FS versus depth profile and PoF versus depth profile for an example location with a slope gradient of 15°. *Red stroke* in the deterministic FS indicates depths with an FS < 1. Modified from Strupler et al. (2017)

the glide plane of the three slides is located in a lithological unit consisting of Late Glacial plastic muds (LU1) corresponding to the sediment-mechanical unit SMU1. The authors stated that future subaqueous slides on the lateral slopes are also expected to occur in this unit. The approach applied by Strupler et al. (2017) can only be used for single-model locations, along seismic reflection profiles. While the glide plane could be determined with a 1D model, the lateral extent of the slides could not be assessed. A grid-based SSA approach needed for a basin-wide subaqueous landslide hazard assessment does not exist so far for Lake Zurich. In this study, we are establishing such a hazard assessment on a spatial scale. In doing so, we differentiate between the probability of failure conditional on geotechnical properties (PoF$_g$), representing the slope-failure susceptibility, and the probability of failure conditional on the earthquake occurrence (PoF$_{eo}$), representing the earthquake-triggered subaqueous landslide hazard. The latter one is calculated by including the seismic hazard in the geotechnical slope-failure probability calculation.

2.4 Probabilistic seismic hazard assessment of Switzerland

Wiemer et al. (2016) provide the latest probabilistic seismic hazard assessment (PSHA) for Switzerland incorporating updates of data, information and knowledge accumulated during the past three decades (e.g. Wiemer et al. 2009). These updates of the 2015 Swiss Seismic Hazard Model (SUIHaz2015) provide probabilistic estimates of horizontal ground motions,

which can be coupled to the response of the local soil characteristics. The ground motions are calculated for a reference site condition with an average shear-wave velocity of the uppermost 30 m of the soil (V_{s30}) = 1100 ms^{-1}. The seismic hazard maps show the spatial distribution of ground motion values corresponding to a fixed probability of exceedance for each computational grid point (Wiemer et al. 2016).

According to Wiemer et al. (2016), earthquake events of magnitude 6–6.5 (hereafter, we refer to as moment magnitude—M_w) are believed to be possible everywhere in Switzerland, albeit they are most frequent in the Valais, the Basle region and the Grisons. A M_w 6 or larger event is expected in Switzerland and its immediate neighbourhood every 50–150 years, thus with an annual probability of about 1%.

3 Methods and workflow

From existing bathymetric, geotechnical and reflection seismic datasets (Strasser and Anselmetti 2008; Strupler et al. 2015, 2017), as final results, back-analysed PoF$_g$ scenarios for different earthquake acceleration scenarios and a basin-wide slope-failure susceptibility
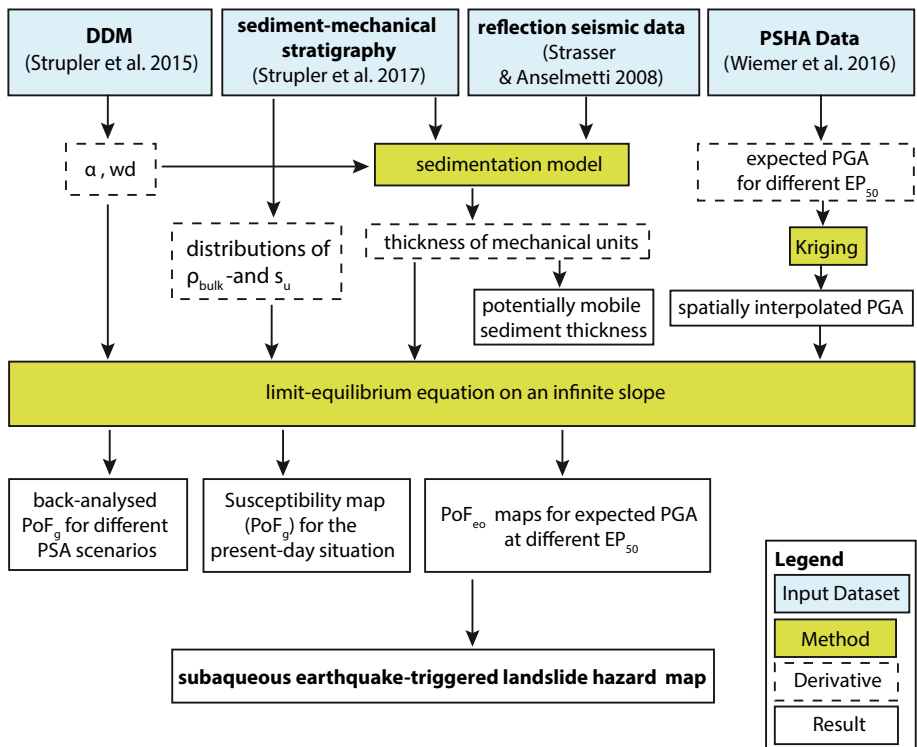
Fig. 4 Workflow for developing the earthquake-triggered, subaqueous landslide hazard map. *DDM* digital depth model, *PSHA* probabilistic seismic hazard analysis; α = slope gradient, wd = water depth, ρ_{bulk} = bulk density, s_u = undrained shear strength, EP_{50} = probability of exceedance in 50 years. PoF$_g$ = probability of failure conditional on geotechnical parameters, PoF$_{eo}$ = probability of failure conditional on earthquake hazard, PSA = pseudostatic acceleration, see Sect. 3.2, PGA = peak ground acceleration

map for the present-day situation are calculated. Furthermore, a subaqueous earthquake-induced landslide hazard map is produced by including the expected ground-shaking data from Wiemer et al. (2016) in the PoF$_{eo}$ calculation (Fig. 4). Calculations are conducted on grids with 10 m spatial resolution in MATLAB (Mathworks, Inc.) and visualized in ArcGIS (ESRI, Inc).

3.1 Sedimentation model

As the grid of the existing seismic reflection profiles (Strasser and Anselmetti 2008) has a spacing between ∼100 and ∼400 m, and as the topography on the lateral slopes of Lake Zurich is complex (Strupler et al. 2015), an interpolation of the sediment-mechanical unit thicknesses, derived from reflection seismic data (Strupler et al. 2017) does not lead to realistic values. Therefore, to extend the thickness information of the mechanical units from locations where reflection seismic data is available to the whole study area, a sedimentation model is constructed (See ESM Figs. 1, 2 for details). The sedimentation model assumes that slopes with comparable settings (e.g. slope gradients, stratigraphic succession) experienced similar sedimentation histories. For SMU3 and 4, the sedimentation rate (sr) at any pixel location (i) is calculated as a function of its water depth (wd) and slope gradient (α) (both derived from the DDM) with a linear regression (Eq. 1, Table 2). The regression equation is calibrated with unit thicknesses from the seismic dataset (divided by the unit age intervals from Strasser and Anselmetti 2008; ∼5000 and ∼7000 years for SMU3 and SMU4, respectively) on two undisturbed transects in the slope that show a wide variety of water depths and slope gradients (ESM, Figs. 1, 2).

$$\text{sr}(i) \text{ [m/year]} = 0.01 * (a(i) \text{ [cm/year]} + b * \text{wd}(i) \text{ [m]} - c * \alpha(i) \text{ [°]}) \tag{1}$$

As unit thicknesses cannot be determined with seismic data, grids with constant values (2.5 and 0.4 m for SMU1 and SMU2, respectively) that are estimated from sediment cores, are constructed for SMU1 and SMU2.

3.2 Limit equilibrium equation on an infinite slope

The limit equilibrium equation on an infinite slope has been applied spatially by several authors (e.g. Dimmock et al. 2012; Hammond et al. 1991; Jibson et al. 2000; Mulder et al. 1994; Terlien 1996). Here, we extend the approach of Strupler et al. (2017), where values of log-normally distributed ρ_{bulk} and s_u were randomly sampled in an MCS for each depth step, and used in a limit equilibrium equation on an infinite slope, to a spatial, grid-based model (Eq. 2). In comparison with other methods, where a pre-defined glide plane is assumed, our approach defines the depth of the glide plane as the depth of the maximum failure probability from all the PoFs per depth step of a PoF-depth profile (Fig. 3b). We assume that the sediment-mechanical conditions from Strupler et al. (2017) that are

Table 2 Regression constants and factors for deriving the sedimentation rate sr(i) as a function of water depth and slope gradient

	a	b	c
SMU4	0.047	0.000175	0.001305
SMU3	0.021	0.000104	0.000654

representing the Oberrieden area (Fig. 1) are also valid for all the slopes surrounding the deep basin. This may be an oversimplification, as the mechanical characteristics may locally vary. However, data from core ZH15-K09 taken at the eastern slope of the basin (Fig. 1) support this assumption, because the lithostratigraphy and the geotechnical profiles show the same patterns and ranges of values (ESM Fig. 5).

The FS versus depth [z (m)] profile at a pixel (i) for each of the 2500 MCS runs is calculated by dividing the resisting forces (dependent on the MCS-selected s_u (Pa) for an undrained case, such as in the water-saturated, fine-grained sediments in our study area) by the downward-driving forces (dependent on the submerged unit weight of the sediment [γ' (N m^{-3})] that itself depends on the MCS-selected ρ_{bulk}-value and the unit weight of water [γ_w (N m^{-3})], the vertical depth [z (m)] below the lake bottom, and the slope gradient (α)). As the infinite-slope model does not account for 'interslice forces' (i.e. shear, compression and tension forces acting between adjacent elements of sediment) on the slope, a pixel-wise FS calculation will typically lead to an underestimation of the FS and overestimation of PoF (Terlien 1996; Dimmock et al. 2012). Therefore, as applied by Dimmock et al. (2012), an additional model bias term (B) is added to the equation. We use $B = 1.25$, as it assigns a deterministic FS of 1 to the pixel groups in the today stable slopes that were characterized by a FS below 1 without the inclusion of a bias term.

$$\text{FS}(i, z, \text{MCS}) = \frac{B * s_u(z, \text{MCS})}{\left(\int_0^z (\gamma'(\text{MCS}))\mathrm{d}z\right) * \sin\alpha(i) * \cos\alpha(i) + \text{PSA}(i) * \left(\int_0^z (\gamma'(\text{MCS}) + \gamma_w)\mathrm{d}z\right) * \cos^2\alpha(i)}$$
(2)

PSA represents the horizontal pseudostatic acceleration (in terms of g), which cannot be compared to the PGA directly, as it only represents a fraction of the PGA (Kramer 1996). Different pseudostatic coefficients k (ranging from 0.05 to 0.5; Melo and Sharma 2004 and references therein) have been applied by different studies. Terzaghi (1951) recommended k-values of 0.1 and 0.2 for 'severe' and 'violent' earthquakes, respectively. Additionally, site amplification (f) for soft sediments ($V_{s30} < 180$ m/s) is $\sim$3 times higher compared to rocks ($V_s > 760$ m/s; Dobry et al. 2000). As the PGA data from the PSHA is calculated for a $V_{s30} = 1100$ m/s, we multiply it in our study with a combined coefficient $k * f = 0.5$, considering both the pseudostatic coefficient (k) and site amplification (f) (Eq. 3).

$$\text{PSA}(\text{soft soil}(i)) = k * f * \text{PGA}(\text{rock}(i))$$
(3)

To investigate the combined effects of k and f on the POF$_{eo}$, a sensitivity test is conducted, assuming that the pseudostatic coefficient k and the PGA amplification by soft sediment (f) cancel each other out, hence $k * f = 1$ (i.e. PSA = PGA; Grilli et al. 2009). The PoF of each depth step per pixel was calculated by dividing the amount of FS values <1 (that were calculated for each MCS run) by the total amount of simulations (2500). Subsequently, maps showing the maximum PoF and corresponding depth of maximum PoF below lake bottom are calculated. Compared to the 1D-SSA approach applied by Strupler et al. (2017), two important changes are implemented in the spatial, grid-based approach: The sediment thickness for the sediment-mechanical units at any pixel (i) in the study basin is estimated with the sedimentation model (Sect. 3.1), and to reduce computation time, the depth sampling rate of the sediment-mechanical stratigraphy is reduced by a factor of 10.

3.3 Back-analysis of the ~2210 cal. years B.P. event

To test the robustness of the model performance and to estimate the strength of the earthquake shaking, we conduct a back-analysis of the $\sim$2210 cal. years B.P. slide in the Oberrieden area (Fig. 2). This slide, with a translation area of $\sim$150,000 m^2, is assumed to be earthquake-triggered, as it occurs coevally with 9 other slides basin-wide (Strasser and Anselmetti 2008; Strupler et al. 2017). The sediment thickness of the drape at the time of failure is calculated with the sedimentation model (for the time $\sim$2210 cal. years B.P.). In order to derive the slope gradient without postslide morphological disturbances (i.e. channels, ridges), the extent of the eroded area is converted from raster to isobaths. The isobaths are smoothed and subsequently interpolated into a new grid, representing a homogenized slide plane. The PoF$_g$ at each depth step at the time $\sim$2210 cal. years B.P. is calculated from FS-distributions (Eq. 2) for given PSA scenarios (i.e. 0, 0.02, 0.04, 0.06 0.08, and 0.1 g), and the failure plane assigned to the depth of the maximum PoF$_g$.

3.4 Assessment of the subaquatic earthquake-induced landslide hazard

The earthquake hazard potential is considered by using the probabilistic peak ground acceleration (PGA) for exceedance probabilities in 50 years (EP$_{50}$) of 10, 2, and 0.5% [i.e. mean return periods (RP) of 475, 2475, and 9975 years]. Spatially distributed PGA values (Wiemer et al. 2016) are spatially interpolated in ArcGIS with the 'Kriging' algorithm, to converge from 10 km to 10 m grid resolution. Subsequently, the high-resolution PGA values corresponding to the different EP$_{50}$ are converted to PSA with Eq. 3 and used in Eq. 2 to calculate PoF$_{eo}$ maps. Finally, these maps are used to assess the subaquatic earthquake-triggered landslide hazard in Lake Zurich.

4 Results

This section provides first the potentially mobile sediment thickness, resulting from the sedimentation model. Next, the results of the back-analysed PoF$_g$ for the $\sim$2210 cal. years B.P. Oberrieden slide are presented. Finally, after showing a slope-failure susceptibility map for the present-day sediment drape, we show the results of the earthquake-triggered subaquatic landslide hazard, given the input of a probabilistically estimated PGA.

4.1 Thickness of the potentially mobile sediment

The cumulative sediment thicknesses of the different SMU visualize the results of the sedimentation model (Fig. 5): In general, the greatest SMU thicknesses can be found in great water depths with gentle slope gradients (such as in the SE-corner of the study area). In shallow, steep zones, only little sediment accumulates, and consequently the smallest SMU thicknesses can be found there. For the basin-wide present-day situation (Fig. 5a), the cumulative thickness of most lateral slopes (gradient 5°–15°) ranges between 5 and 8 m. Basin-wide thicknesses of SMU3 and SMU4 vary between 0 and 1.8 and 0 and 4.8 m, respectively (ESM, Fig. 3). While at the time of the $\sim$2210 cal. years B.P. slide, between $\sim$4 and $\sim$7 m of sediment was available on most parts of the slopes (Fig. 5b), up to $\sim$1.5 m of sediment have been deposited on the slopes since that time (ESM, Fig. 4).
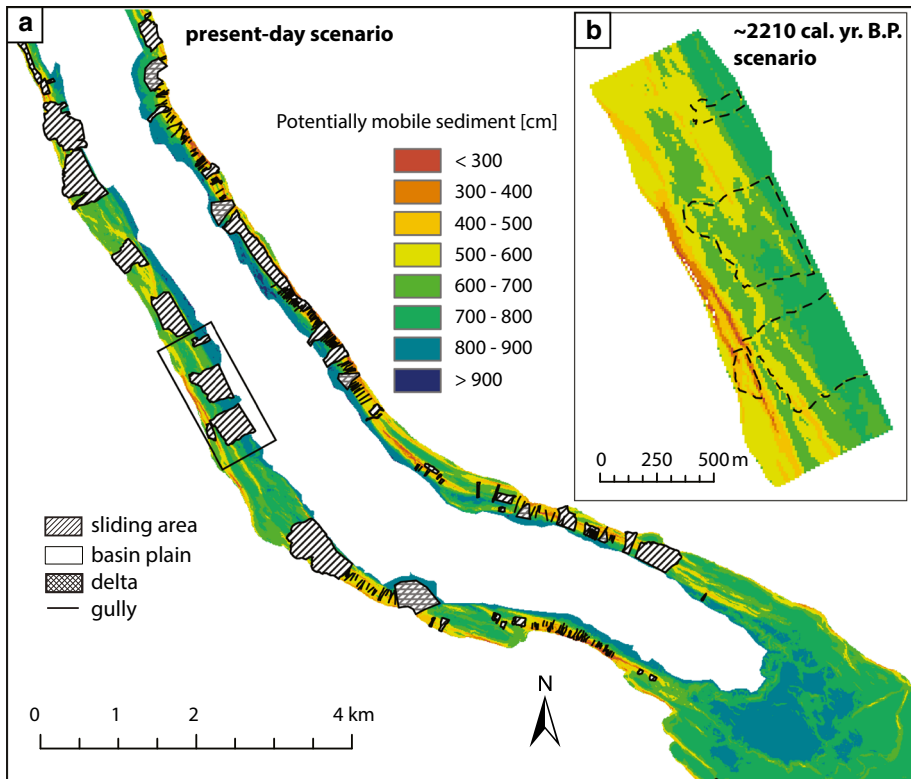
Fig. 5 Cumulative thickness of the potentially mobile sediment-mechanical units for the present-day situation (**a**) and the scenario ∼ 2210 cal. years B.P. (**b**)

4.2 Back-analysed PoF$_g$ for the ~2210 cal. years B.P. landslide in Oberrieden

Grid-based PoF$_g$ for the sediment drape at the time of the ∼ 2210 cal. years B.P. event, calculated for different pseudostatic accelerations, are shown in Fig. 6. For a static situation (i.e. no external load) no major group of pixels with a PoF$_g$ of greater than 0.2 can be found (Fig. 6a), indicating a generally stable slope. Whereas for PSA scenarios 0.2 and 0.4 g, a great part of the slope shows a low PoF$_g$ (0–0.2) and only isolated zones have a PoF$_g$ greater than 0.4, PoF$_g$ become generally high (i.e. >0.6) for PSA scenarios higher than 0.6 g (Fig. 6d–f). For a PSA of 0.08 g, the northern and southern parts of the Oberrieden slope shows a lower PoF$_g$ towards the shore, while the central part of the slope shows high PoF$_g$ (0.6–1) from nearshore to the toe of the basin. For a PSA scenario of 0.1 g, practically the whole slope has a PoF$_g$ between 0.8 and 1.

A multiplication of the sum of the depth of the maximum PoF$_g$ of all pixels (ESM, Fig. 6.) with the cell size leads to a mobilized slide volume of the ∼ 2210 cal. years B.P. slide in the range between ∼ 583,000 and 818,000 m^3 (Table 3).
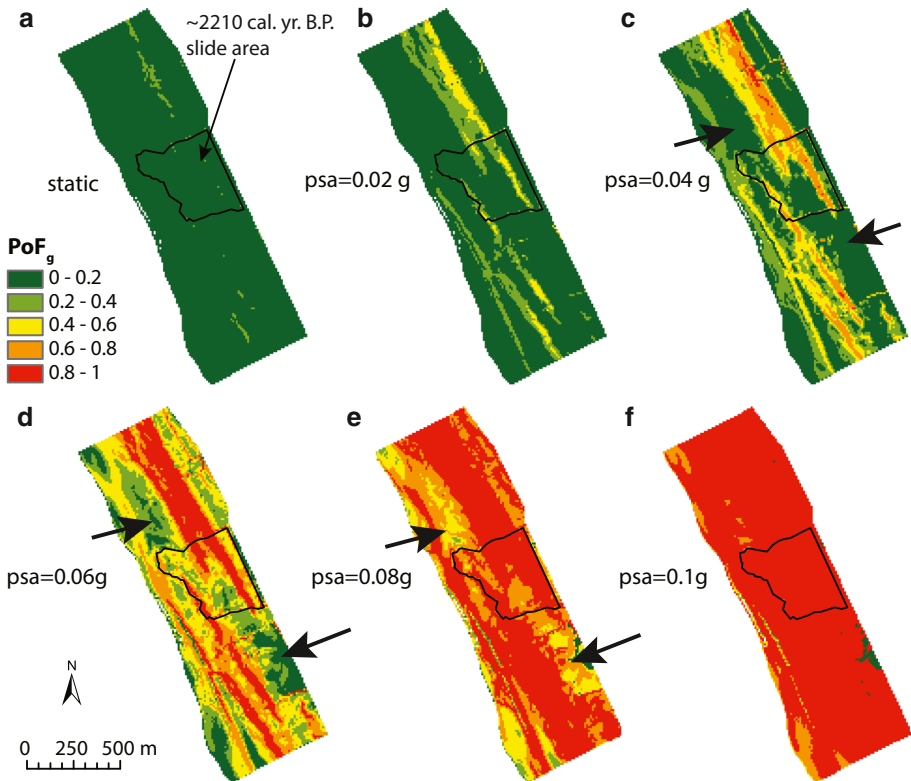
Fig. 6 Different pseudostatic earthquake acceleration scenarios (PSA = 0, 0.02, 0.04, 0.06, 0.08 and 0.1 g) for the Oberrieden slope at the time ∼2210 cal. years B.P. resulting in different PoF. *Black polygon* shows extent of the ∼2210 cal. years B.P. slide

Table 3 Modelled slide volumes for selected PSA scenarios presented in Fig. 6

PSA scenario (g)	Modelled slide volume (m^3)
0.04	582,900
0.06	803,900
0.08	817,500

4.3 Basin-wide slope-failure susceptibility of the static present-day situation

A basin-wide SSA for the present-day situation under static loading conditions show that 87% of the studied slopes have a PoF_g of <0.2, 8% a PoF_g between 0.2 and 0.4, 4% a PoF_g between 0.4 and 0.6, and 0.5% have a PoF_g between 0.6 and 0.8 and 0.8–1, respectively (Fig. 7). Most of the pixel aggregations with a PoF_g >0.4 occur on the steep slopes, where gullies occur. Only a few steep zones without gullies, located mostly in midslope or downslope positions show a relatively high PoF_g (0.4–0.6). An interpretation of such relatively high static PoF_g is provided in the discussion section.
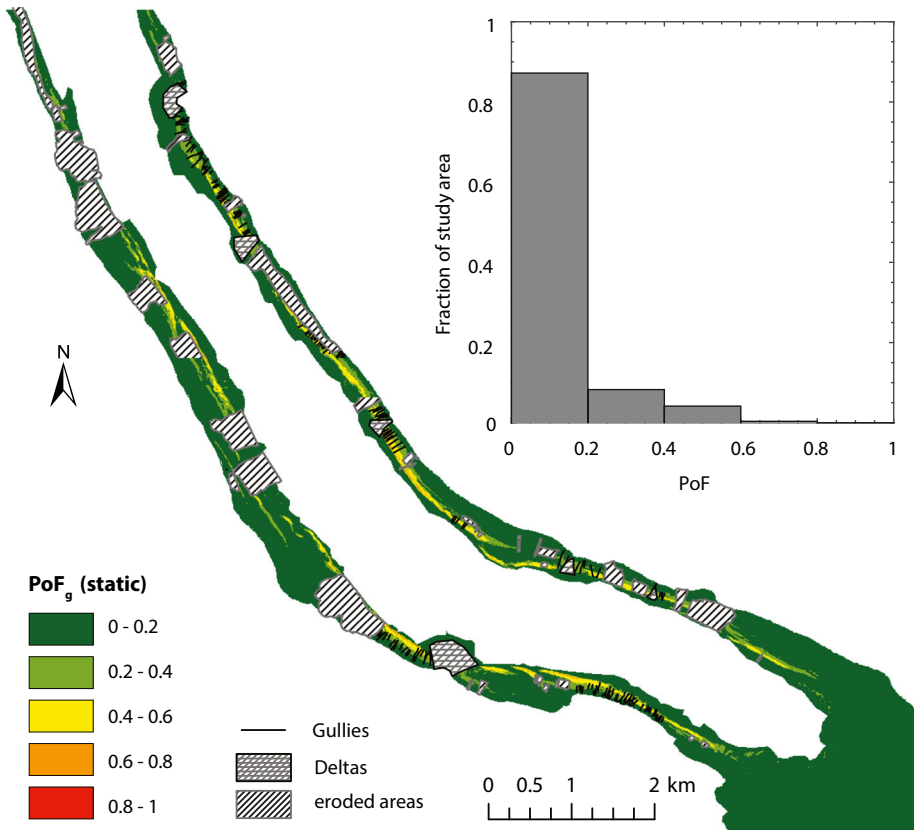
Fig. 7 Slope-failure susceptibility map for the present-day situation for a static case (i.e. no external trigger)

4.4 Earthquake-triggered, basin-wide subaqueous landslide hazard

4.4.1 Spatially interpolated ground-shaking values (PGA)

The reference hazard curve for Oberrieden gives the exceedance probabilities of various levels of PGA in 50 years. Median and two percentiles (5th and 95th) as provided by the 2015 updates of the Swiss Hazard Model (Wiemer et al. 2016) are illustrated in Fig. 8a. The horizontal black-dashed lines represent the considered EP_{50} and their corresponding PGA values (vertical black-dashed lines). Note, the smaller the EP_{50}, the greater the expected PGA values (Fig. 8).

In the whole study area, the median PGA values vary around ~ 0.05, ~ 0.1 and ~ 0.2 g for EP_{50} of 10, 2 and 0.5%, respectively. Values are slightly higher in the south-eastern than in the north-western part of the basin, due to proximity to the Alps (Wiemer et al. 2016).
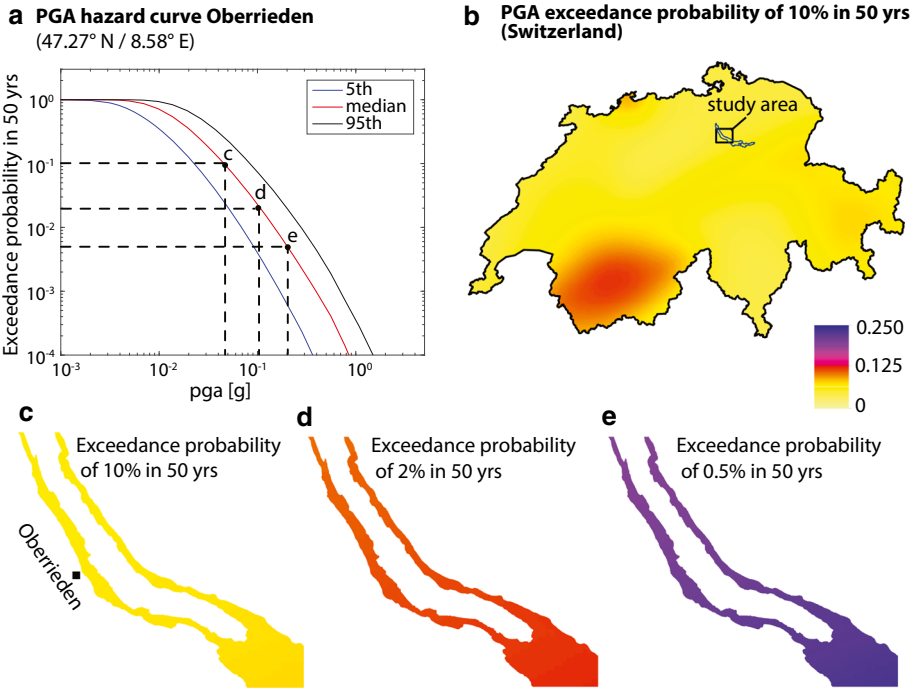
Fig. 8 **a** Seismic hazard curves for Oberrieden as provided by the 2015 Swiss Seismic Hazard Model (Wiemer et al. 2016). **b** Reference hazard map depicting PGA values for exceedance probabilities of 10% in 50 years. The study area is marked with *a black rectangle*. The spatial distributions of PGA for exceedance probabilities of 10, 2 and 0.5% in 50 years for the lateral slopes of Lake Zurich are shown in (**c–e**). Switzerland borders: swisstopo

4.4.2 Basin-wide PoF_{eo} for PGA levels at different EP_{50}

In general, the PoF_{eo} increases with larger PGA values, which can be expected with smaller exceedance probabilities (Figs. 8, 9). PGA values for an EP_{50} of 10% cause a high PoF (i.e. >0.6) at the steeper zones of the slope ($\sim 20°$). Relatively gentle slopes (<10°) show a low PoF (i.e. <0.2) for a PGA with an EP_{50} of 10% (Fig. 9a). For PGA values with an EP_{50} of 2%, only the gentle slopes (i.e. gradients < $\sim 5°$) show low to medium PoF_{eo} values (i.e. 0.4; Fig. 9b). For PGA values with an EP_{50} of 0.5%, all lateral slopes show a PoF between 0.8 and 1 (Fig. 9c).

The PoF_{eo} for selected locations with different slope gradients (indicated in Fig. 9 with white asterisks), plotted against median PGA for different mean RP are shown in Fig. 10. The blue and black curves, representing low slope gradients (of 1° and 7°, respectively), show a slower increase in PoF_{eo} with increasing mean RP than a medium slope gradient (12°, red curve). For slopes with steep gradients ($\sim 20°$, green curve), however, the PoF_{eo}, increases slower with PGA values for higher mean return periods. This suggests a non-linearity between the involved factors slope gradient, water depth and thickness of the SMUs, which are also dependent on the slope gradient and water depth (c.f. sedimentation model), leading to the calculation of the PoF_{eo}. For steep slopes (20°, green curve), the slope gradient (and thus gravity) has a stronger influence on the PoF_{eo} than the PSA. This results from the applied limit equilibrium equation on an infinite slope, where the PSA is
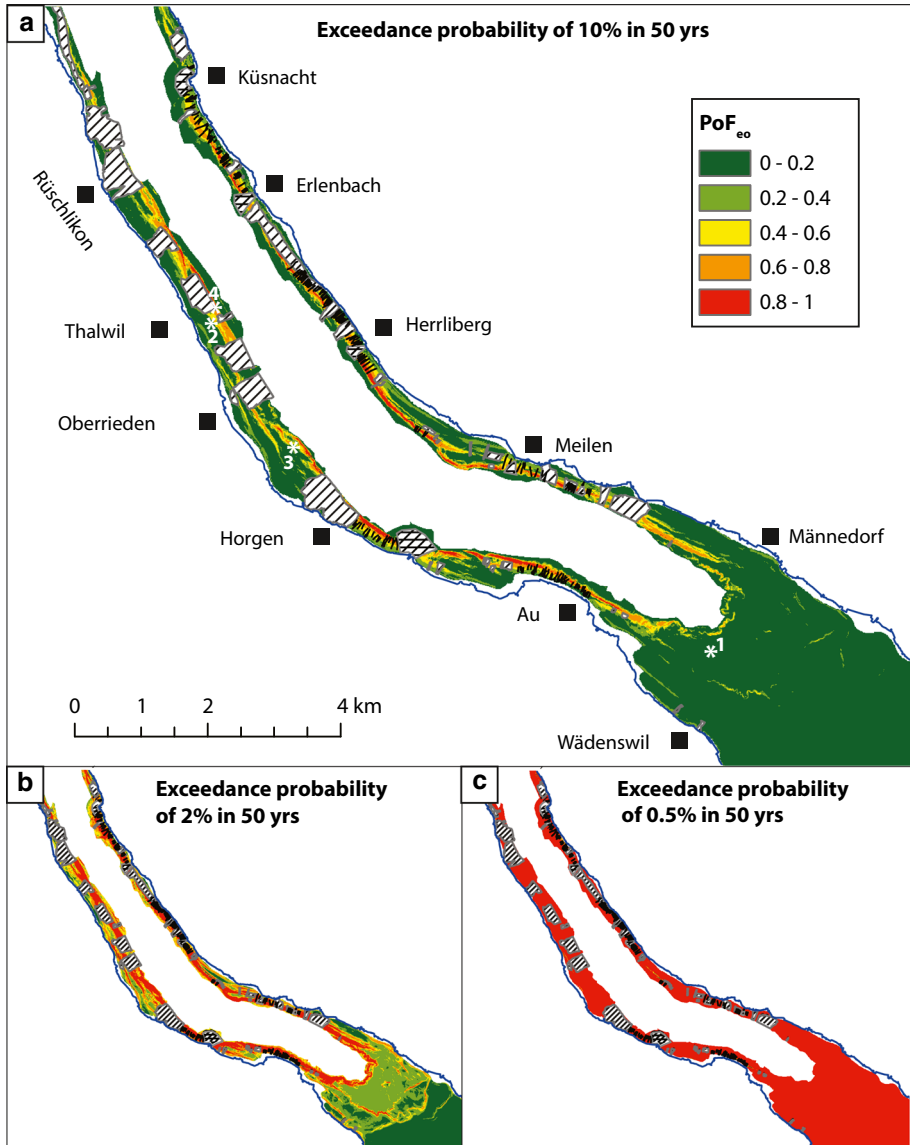
Fig. 9 PoF$_{eo}$ of each pixel given the forecasted, pixel-wise PGA (median) exceedance probabilities (c.f. Fig. 8) from the PSHA. Shorelines: swisstopo

multiplied by the cosine of the slope, hence the steeper the slope, the smaller the influence of the PSA (i.e. cos 0° = 1 and cos 90°; scenario of a vertical slope = 0). Figure 10 also shows that for a mean RP of 9975 years (i.e. EP$_{50}$ of 0.5%), the PoF$_{eo}$ equals 1 for the selected locations. As the maximum PoF$_{eq}$ is per definition 1 (i.e. 100%), the data points for a RP of 9975 years (i.e. EP$_{50}$ of 0.5%) that show all a PoF$_{eq}$ of 1 are not following the expected linear fit for the same slope gradient, manually continued with a dashed line in the semi-logarithmic plot (Fig. 10).
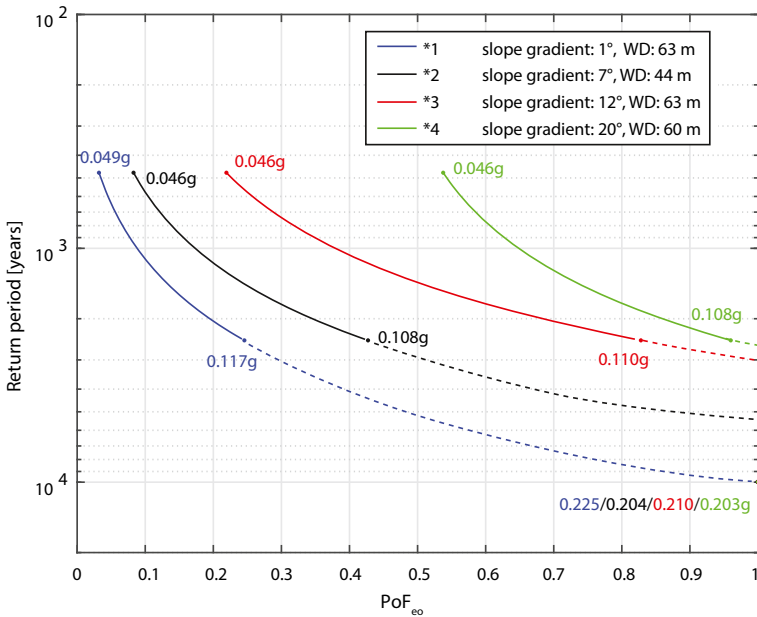
Fig. 10 PoF_{eo} versus forecasted median PGA for different return periods at four selected locations with different slope gradients. The locations are indicated with *white asterisks* in Fig. 9 (*dashed line* is manually continued). *Points* are labelled with their local PGA values corresponding the respective EP_{50}

5 Discussion

In this section, we discuss the results presented in the previous chapter in the context of the research questions posed in Sect. 1.

5.1 Potentially mobile sediment on the lateral slopes

The water depth and slope gradient have a great influence on the estimated sedimentation rate: The greater the water depth, the more sediment, and the steeper the slope, the less sediment. This is consistent with dynamic processes along steep slopes, where hemipelagic sediment settled through the water column is not deposited but directly re-mobilized due to gravity and deposited at the foot of the slope. Due to the fact that the glide planes of the investigated slides in a previous study did not occur at a boundary between two sediment-mechanical units but rather within SMU1 (Strupler et al. 2017), the cumulative thickness of the sediment-mechanical units overestimates the potentially mobile sediment (as it accounts the whole SMU1 to the slide depth). Hence, we consider the potentially mobile sediment volume from the calculated depth of the modelled slide surface, characterized by the highest PoF value (ESM, Figs. 6, 7). The potentially mobile sediment volume is discussed for the back-analysis in Sect. 5.2 and for the present-day hazard assessment in Sect. 5.3.

5.2 Back-analysed PoF$_g$ of the ~2210 cal. years B.P. slide for different PSA scenarios

The PoF$_g$ <0.2 for a static scenario (Fig. 6a) indicates a low probability of a spontaneous failure (i.e. without additional trigger) for the reconstructed sediment drape thickness at the time of the ~2210 cal. years B.P. subaqueous landslide offshore Oberrieden. This supports the hypothesis by Strasser and Anselmetti (2008) of an earthquake as trigger for the ~2210 cal. years B.P. event. A PSA between 0.04 g (Fig. 6c) and 0.08 g (Fig. 6e) seems the most plausible for explaining the triggering of the 2210 cal. years B.P. event. The lower PSA limit can be constrained as many pixels in the area where the slide occurred show values with a PoF$_g$ of between 0.6 and 1. The upper PSA limit can be constrained by the fact that a PSA of >0.08 g would effect in a PoF$_g$ of 0.8–1 for almost all pixels of the slope, which would most probably have resulted in a larger, slope-wide subaquatic slide. Converting the PSA values to PGA values with a $k * f$ value of 0.5, PGA values between 0.08 and 0.16 g are suggested for the ~2210 cal. years B.P. event (Eq. 3), approximating the expected PGA values for an earthquake with an EP$_{50}$ of 2% (RP of 2475 years). The back-calculated values by Strasser et al. (2007) for the ~2220 cal. years event in neighbouring Lake Lucerne show a similar range (PGA = 0.06–0.16 g) as from our determination.

The modelled slide volume for a PSA scenario of 0.04 g (~583,000 m^3) is slightly lower than the first-order estimated volume (~750,000–1,050,000 m^3) by Strupler et al. (2017). This PSA scenario assigns a low depth of glide plane to the zones with a low PoF (Fig. 6; ESM Fig. 6) and might thus underestimate the slide volume. However, both calculated volumes of the slide for a PSA of 0.06 and 0.08 g (Table 3) are within the range of the volume estimated by Strupler et al. (2017).

An exact determination of the lateral extents of the slides on the basis of the slope-stability modelling is not conclusive, because both high and low PoF$_g$ values are calculated for the area inside and outside of the slope portion that failed during the ~2210 cal. years B.P. event. No clear pattern can be recognized from the PoF$_g$ distribution that would allow to correctly predict the lateral extent of the landslide. However, it seems that the lateral extent of the ~2210 cal. years is defined by a continuously high PoF throughout the slope (i.e. from the top to the toe of the slope), caused by local slope-gradient characteristics. The more gently inclined zones with a lower PoF to the north and south of the translation area of the slide (marked with arrows in Fig. 6) may have prevented the partially unstable zones of the slope to fail. A more sophisticated model would be needed to assess the exact slide extents (e.g. Bellugi et al. 2015). In conclusion, the back-analysis of the ~2210 cal. years B.P. slide offshore Oberrieden can be regarded as a proof of concept, as the estimated PSA values are in the range of similar events, the modelled slide volume is in the same range as estimations with other methods (Strupler et al. 2017), and as the slide occurred on areas with high calculated PoF$_g$ values.

5.3 Subaqueous landslide hazard in Lake Zurich

5.3.1 Basin-wide subaquatic slope-failure susceptibility (PoF$_g$) for the present-day situation

Most parts of the slopes have a low PoF (i.e. <0.2), indicating stable conditions for the present-day situation under static loading, i.e. without external trigger (Fig. 7). According

to our model, the zones with steeper slope gradients (i.e. >25° in Fig. 1) with a medium PoF$_g$ (i.e. 0.4–0.6) are susceptible to failure for a static case. Due to the fact that gullies in Lake Zurich occur on most of these steep parts of the slope, and that no major landslide deposits can be found at the bottom of the lake below the gullied slopes, we assume that these gullies act as pathways of sediment transport (Field et al. 1999), as the slope is too steep for a considerable sediment accumulation. A subsequent failure of these parts of the slopes is thus very unlikely, suggesting the model is not valid on these steep slopes (>25°). Different mechanisms have been proposed for the formation of such gullies, e.g. slope-parallel bottom currents, sediment-gravity currents, among others (e.g. Field et al. 1999; Izumi 2004; Sultan et al. 2004; Fedele and García 2009; Micallef and Mountjoy 2011).

The assumption of constant SMU1 and SMU2 thicknesses may also contribute to the relatively high static PoF$_g$ on the above mentioned slopes. For the few steep parts of the slopes, where no gullies occur, it cannot be excluded that spontaneous failures without an earthquake trigger occur. However, as their downslope length is often relatively short compared to the whole slope, they might be buttressed by the surrounding sediment. Also, landslides are mostly expected on slopes where greater accumulations of pixels with high PoF are found (Terlien 1996), thus such smaller zones with high PoF$_g$ may not be enough to trigger landslides.

5.3.2 Earthquake-induced landslide hazard

While landslide susceptibility maps show areas where future landslides are expected to occur, a landslide hazard map includes the probability of their occurrence within a given observational time, e.g. described by the exceedance probability in 50 years (EP$_{50}$). The earthquake-triggered subaquatic landslide hazard has been assessed and discussed with different methods in the past (Urgeles et al. 2002; Grilli et al. 2009; Strasser et al. 2011; Dimmock et al. 2012). A novelty of our approach, which combines data from a high-resolution sediment-mechanical stratigraphy (Strupler et al. 2017) integrated in spatial PoF$_g$ analyses with probabilistically estimated ground motions (Wiemer et al. 2016), is that the hazard is directly calculated as PoF$_{eo}$ (Fig. 9). Plotting the PoF$_{eo}$ as function of the mean return periods represents a novel tool to facilitate communicating the landslide hazard. To our knowledge, this constitutes one of the first sublacustrine earthquake-triggered landslide hazard maps (Fig. 9). The proposed methodological approach may also be applied for slopes in the marine realm.

For a forecasted median PGA for a EP$_{50}$ of 10% (i.e. PGA values of ∼0.05 g), slopes with gradients >20° become unstable (PoF$_{eq}$ > 0.6; Figs. 9, 10, 11). The comparably twice as high median PGA values expected for an EP$_{50}$ of 2% (i.e. PGA values of ∼0.1 g) would cause, under today's sediment load, most slopes greater than ∼10° to fail. The ∼2210 cal. years B.P. event mapped by Strasser and Anselmetti (2008) might represent such an event with an EP$_{50}$ of 2% (RP 2245 years), as 10 basin-wide large mass failures are assigned to it, but not all lateral slopes failed coevally (which would rather suggest an earthquake with an EP$_{50}$ of 0.5%). However, because of the up to ∼1.5 m thinner sediment drape at that time, in general the Oberrieden slope was more stable ∼2210 cal. years B.P. than it is at present. This means that some previously (i.e. 2210 cal. years B.P.) stable areas would fail at present for PGA scenarios with the same EP$_{50}$. Our model indicates that an earthquake with a EP$_{50}$ of 0.5% (RP of 9975 years), would cause the simultaneous failure of all slopes (Figs. 9, 10, 11). We do not have any evidence for a coeval failure of all lateral slopes in the bathymetric nor in the seismic reflection datasets, covering timescales of the past 5000 and ∼17,000 years, respectively (Strasser and Anselmetti 2008; Strupler et al. 2015).

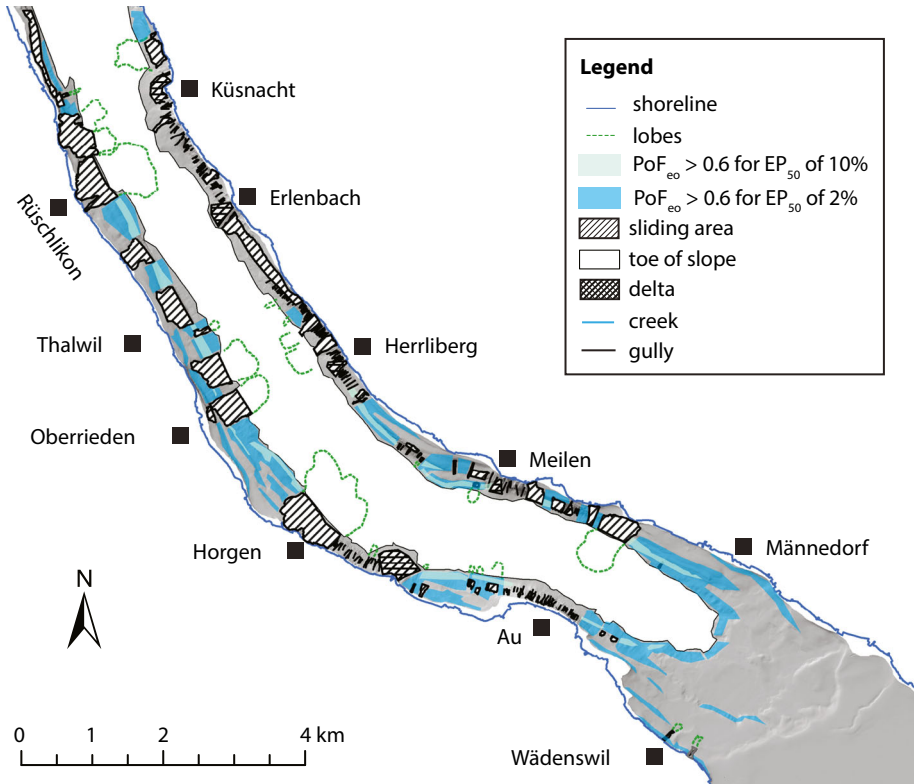**Fig. 11** Mapped most probable slide scenarios for EP_{50} of 10 (*light blue*) and 2% (*dark blue*): $PoF_{eo} > 0.6$ for EP50 of 0.5% is not mapped for illustrating reasons, as it covers all yet unfailed slopes

However we do not exclude such a strong earthquake with PGAs of an EP_{50} of 0.5% since deglaciation. As the lacustrine chalks (SMU3) and marls (SMU4) were only deposited in the last ~12,000 years (Strasser and Anselmetti 2008) and thus before then, no SMU3 and SMU4 were draping the Late Glacial plastic muds (SMU1). This means that the sediment load on today's weak layer (SMU1) must have been much lower back then. Therefore, the sublacustrine slopes might have stayed stable during a relatively strong earthquake in the beginning of the Holocene.

The absolute depth (within the sediment column) of the maximum PoF_{eo} for each pixel depends on the external load applied to the sediment column by the earthquake (ESM, Fig. 7). For relatively gentle dipping slopes (<5°) with little earthquake loading, the maximum PoF_{eo} can be found in the uppermost dm of the sediment column, caused by the higher variability of the s_u-data in the uppermost layers (Strupler et al. 2017). For medium to steep slopes (>15°), or for relatively gentle slopes with increased earthquake loading, this uppermost increased PoF_{eo} does not represent the maximum PoF_{eo} of the PoF_{eo} versus depth profile anymore, as the increasing horizontal component of gravity force and the resulting increased PSA value shift the maximum PoF_{eo} to SMU1. For moderate and steeper parts of the slope, the potential glide plane is always located in SMU1 (Late Glacial plastic muds). For the comprehensive SSA, we consider the fact that the maximum (albeit very low) PoF_{eo} on such gentle slopes is located in the uppermost dm of the sediment

column as not relevant, as it is rarely greater than 0.2. Also, the maximum PoF_{eo} in the uppermost dm of the sediment column indicates that the PoF in SMU1 must be even smaller on such flat slopes. Based on the maps displaying the subaqueous earthquake-triggered landslide hazard, the individual zones of potential future landslides are mapped manually. In the following paragraphs we show and discuss potential landslide zones for a PoF_{eo} >0.6, excluding deltaic and zones and gullies (Fig. 11). This threshold value was selected in order to map the most probable areas of landslides. A pixel-wise multiplication of the zonal potential landslide area with the depth of the maximum PoF_{eo} for different EP_{50} leads to an estimation of potential landslide volumes.

For an earthquake with an EP_{50} of 10%, a maximum basin-wide landslide area of $\sim 600{,}000$ m^2 and maximum volume of ~ 3 Mio m^3 is expected, if all considered slopes failed simultaneously ('worst-case scenario'; ESM, Table 2). Most of the areas on the slopes presently prone to failure show potential translation areas that are smaller than the past slide areas, mapped in Strupler et al. (2015). These zones are mostly located midslope, especially on the northeast-facing slopes between the villages of 'Rüschlikon' and 'Thalwil' (potentially mobile volumes of $\sim 540{,}000$ m^3). The zone just north of the Horgen slide (Heim 1876; Kelts and Hsü 1980) is considered as relatively stable for an PGA with an EP_{50} of 10%. An earthquake with an EP_{50} of 2% (i.e. RP of 2475 years), may trigger landslides with a cumulative area and volume of ~ 2.2 Mio m^2 and ~ 12 Mio m^3, respectively. In particular, failure-prone slopes are located between 'Rüschlikon' and 'Thalwil', in the zone south of the 1875 Horgen slide and north of Au (each with potentially mobile volumes of up to ~ 1.9 Mio m^3), and between 'Meilen' and 'Männedorf' (potentially mobile volumes of 4.3 Mio m^3; ESM, Fig. 8, Table 3). For a scenario of an earthquake with an EP_{50} of 0.5%, a maximum cumulative sliding area and volume of ~ 13 Mio m^2 and ~ 70 Mio m^3, respectively, is estimated. The greatest potentially mobile sediment volumes for an EP_{50} of 0.5% are located at the geomorphic escarpment structure, separating the deep basin from the shallower basin to the south (Fig. 1), where slope gradients are very low, indicating a low potential slide velocity.

Concluding, the slopes most prone to failure in Lake Zurich are the ones with a gradient between $\sim 10°$ and $\sim 25°$ (Fig. 11). This is also the slope range where most of the identifiable slides in the DDM occurred during the last ~ 5000 years (Strasser et al. 2013; Strupler et al. 2015). A similar range of slope gradients was identified as failure-prone by Strasser et al. (2011) for Lake Lucerne. The earthquake-induced landslide hazard should not be ignored, as most of the yet unfailed lateral slopes contain parts with a very high seismic landslide hazard. While for EP_{50} of 10 and 2% the amount of relatively small, individual slides is high, for EP_{50} of 0.5%, landslides with much greater extent and volumes are estimated. These maximum cumulative potential slide volumes for the different EP_{50} scenarios should be considered as worst-case scenarios, as all the mapped slides would occur coevally.

Disaggregation of seismic hazard at a given location provides the tool to identify controlling (i.e. most likely) scenarios for specific ground motion levels. We disaggregate the seismic hazard at the location of the deepest point of the central basin for the different mean return periods (i.e. 475, 2475 and 9975 years). The controlling scenarios—defined by M_w and distance (R) in km, are: $M_w = 4.7$ and R 12.5 km for a mean return period of 475 years, $M_w = 4.7$ and R 7.5 km for a mean return period of 2475 years, and $M_w = 5.1$ and R 7.5 km for a mean return period of 9975 years (ESM, Figs. 10, 11, 12).

5.4 Limitations and quality of our approach

Since the earliest attempts of slope-stability assessments (SSA), engineers have been plagued with discrepancies in the results obtained (Bertoldi 1988). The scope of this study was not to provide the absolute numbers of failure probability. Rather, we present a new approach for the assessment of the subaqueous, earthquake-induced landslide hazard in subaqueous settings. The results should thus be considered as a first-order estimation, due to the above mentioned limitations of the methods used in the analysis. However, the here presented subaquatic landslide hazard map indicates parts of the slopes that are more prone to failure than others, which is valuable information, especially for estimating the consequences of potential slides.

Our results build on various datasets, each including uncertainties. The geotechnical uncertainties are considered by a Monte Carlo sampling of the input values, and the uncertainties concerning earthquake accelerations are respected in the PSHA of Wiemer et al. (2016). Nevertheless, our approach still contains some limitations, including the following points:

- As already mentioned in Strupler et al. (2017), the assumption of the infinite-slope mode that the glide plane is planar, is not strictly valid for the slopes of Lake Zurich (Switzerland), which show an irregularly changing bathymetry. Also, using a pseudostatic approach, where a constant force acting only in one direction is applied to the sediment column does not consider the earthquake shaking history (e.g. Jibson 2011). A strong shaking for a very short time does not necessarily need to cause failure, which is not considered in the here used pseudostatic approach, implying only first-order estimations of slope stability. As the constant pseudostatic force, represented by the peak ground acceleration, acts only briefly, a pseudostatic coefficient is selected. However, the selection of such a pseudostatic coefficient is difficult although critically important (Bray and Travasarou 2009; Jibson 2011). The coefficient also depends on the fundamental period (Ts) of the sliding mass, which is calculated by the division of four times the height of the sliding mass (H) by V_{s30} of the sediment (e.g. Bray and Travasarou 2009, Eq. 4):

$$Ts = \frac{4H}{Vs_{30}} \tag{4}$$

  Due to missing information on the V_{s30} of Lake Zurich's sediments, and because literature values for subaqueous and mainly silty-clayey soils show V_{s30} values in the range between <100 and 400 m/s (e.g. Ewing et al. 1992; European Commitee for Standardization 2004; Hunter et al. 2007; Vessia et al. 2015), these values could not be calculated. The influence of the seismic coefficient and the PGA amplification on the PoF_{eo} is demonstrated in a sensitivity test (ESM, Fig. 9), where it is assumed that k and f cancel each other out ($k * f = 1$), thus PSA is assumed equal to PGA in that case and consequently, the PoF_{eo} is much higher. For example, while most of the slopes show a low PoF_{eo} (i.e. <0.4) for PGA forecasted for an EP_{50} of 10%, assuming $k * f = 0.5$, most of the slopes show a high PoF_{eo} (i.e. >0.6) for $k * f = 1$.
- A calculated high PoF, which implies slope failure, does not necessarily mean that a landslide will result immediately. As a first stage of unstable slopes, some local deformations of the sediment on the slopes may occur (e.g. Leroueil et al. 1996; Shillington et al. 2012).

- Another limitation is that our approach does not consider possible hydrological effects. However, as deltas are excluded in our SSA, and no fluid flow evidence can be found in the geoacoustic datasets, we consider such effects not relevant for Lake Zurich. The exclusion of deltas, however, may underestimate the landslide hazard, as delta failures can happen even without additional triggers (e.g. Girardclos et al. 2007), mainly because of high sediment input. Strasser and Anselmetti (2008) mapped a mass transport deposit at the base of the Küsnacht Delta (Fig. 1), documenting such a delta collapse. In future studies, delta collapses should be included in subaqueous hazard assessments.

- The quality of the sedimentation model can be independently controlled with the thickness of the sediment-mechanical units from cores (ESM, Table 1; Strasser and Anselmetti 2008; Strupler et al. 2017). Due to positioning uncertainties during coring, vertical uncertainty in reflection seismic data and local sedimentation rate variations, the sedimentation has some uncertainties. There is no clear trend identifiable, for which slope- and water-depth characteristics the error is greatest. The mean deviation between the calculated and the measured sediment thickness is smaller than 10% for both SMU3 and SMU4. Also, uncertainties in age intervals of the sediment-mechanical units ($\pm \sim 200$ years for bottom SMU4 and ± 400 for the bottom of SMU3) affect their thickness. However, this uncertainty affects changes in the sediment column by variations of ~ 1 dm and is thus smaller than the influence of the above mentioned other uncertainties. We assume a constant sedimentation rate for the time intervals during SMU3 and SMU4. An age model from Strasser and Anselmetti (2008), however, indicates that while during deposition of SMU3, the sedimentation rate remained more or less constant, sedimentation rate was slightly greater in the last ~ 1000 cal. years B.P. This provides another uncertainty for the thickness of the sediment drape at the time ~ 2210 cal. years B.P.

- Our model is not valid for slopes with gradients >25°. However, as on most of these slopes gullies occur that inhibit sedimentation by directly transporting the sediment to the toe of the slope, these steep zones are regarded to remain stable, as no potentially mobile sediment is available.

In general, it is difficult to judge the quality of a hazard assessment, as a predicted hazard can only be verified or falsified by its occurrence or not-occurrence (Heinimann et al. 1998). However, the fact that the already failed slopes in the study area are surrounded by zones with a high slope-failure susceptibility motivates the usefulness of our approach. The results of the back-analysis at the case-study site 'Oberrieden' can be regarded as 'proof of concept', although they also show the limitations in predicting the exact lateral extent of landslides. The back-analysis as well as the slope-failure scenarios from the hazard assessment of the present-day situation, suggest that a PGA with an EP_{50} of 2% (i.e. mean recurrence time of ~ 2475) years characterize the ~ 2210 cal. years B.P. prehistorical event.

5.5 Outlook

Hazard assessments should be an ongoing process (Wang et al. 2005), which need updates if changes in the input parameters occur. Ongoing sedimentation will increase the hazard (by adding more sediment load on the slopes) whereas removal of sediment by future landslides will decrease the subsequent hazard. In a future work, it may be investigated whether the documented landslides on the lateral slopes of Lake Zurich were capable of

triggering tsunamis and, if that is the case, they could be quantified. Also, based on the here presented subaquatic earthquake-triggered landslide hazard map, a tsunami hazard assessment may be conducted.

Furthermore, the earthquake-triggered hazard may be assessed with the spectral acceleration as a function of the fundamental period of the soil, instead of PGA, to include resonance. To achieve this, knowledge of V_{s30} of the sediments on the lateral slopes is required.

Regarding the mechanism of slope failures in nearshore areas, there is a general lack of knowledge. For assessing the shore loading induced landslide hazard, an approach that combines onshore and offshore data is needed (L'Heureux et al. 2013). For example, small subsidences caused by shore loading may be detected by remote sensing techniques, such as differential SAR interferometry. As the shores of Lake Zurich are densely populated, potential shore collapses always pose a threat to infrastructure along the shore.

6 Conclusions

We present an approach for the basin-wide earthquake-induced subaquatic landslide hazard assessment, based on high-resolution sediment-mechanical and geophysical input data. Furthermore, we provide a first quantitative landslide hazard estimation for the lateral slopes in Lake Zurich. To this end, a sedimentation model is calibrated from sediment cores and seismic data, to map the thicknesses of the sediment-mechanical units. Parts of the slopes in greater water depth and low slope gradients show the greatest thicknesses of the mechanical units. The mapped sediment-mechanical unit thicknesses were used in a spatial limit equilibrium model on an infinite slope, with Monte Carlo sampled input values from log-normally distributed mechanical properties of the lateral slopes from a previous study (Strupler et al. 2017).

The following outcomes are highlighted:

- A back-analysis for the ~2210 cal. years B.P. Oberrieden landslide revealed pseudostatic critical accelerations in the range of 0.04–0.08 g (corresponding to PGA values between ~0.08 and 0.16 g). This acceleration is comparable to back-calculated values of the ~2220 cal. years B.P. in Lake Lucerne.
- In terms of hazard, the ~2210 cal. years B.P. event in Lake Zurich can be assigned to an earthquake with an exceedance probability of 2% in 50 years (median PGA values of ~0.1 g). A similar earthquake happening for the present-day sediment drape is assumed to cause failure at zones that remained stable during the ~2210 cal. years B.P. event, due to a change stability conditions, caused by additional sediment loading.
- A hazard evaluation of the present-day sediment drape indicates that an earthquake with a probability of 10% in 50 years (median PGA of ~0.05 g) may be sufficient to trigger multiple, yet minor subaqueous landslides on the lateral slopes of Lake Zurich. An earthquake with an exceedance probability of 2% in 50 years (median PGA of ~0.1 g) might cause major failures on the lateral slopes, where as an earthquake with an exceedance probability of 0.5% in 50 years (median PGA of ~0.2 g) might be considered as 'worst case' scenario, where all slopes are supposed to fail (estimated volume ~70 Mio m^3).
- Generally, for earthquakes with ground accelerations forecasted for exceedance probabilities of 10 and 2% in 50 years, the slopes most prone to failure have gradients between 10° and 25°. Such slopes can mostly be found (1) between the villages of

Thalwil and Rüschlikon with potential failure volumes of $\sim$540,000 and 1,900,000 m^3 for an exceedance period of 10 and 2% in 50 years, respectively, (2) south of the 1875-Horgen slide (with potential failure volumes of $\sim$490,000 and 1,900,000 m^3) and (3) between Meilen and Herrliberg with potential failure volumes of $\sim$440,000 and 4,320,000 m^3).

It is obvious that subaqueous landslides in Lake Zurich will occur in the future. Hence, it is important to estimate where and when they will occur, and what threat they pose to society. While we cannot control most of the factors determining the landslide hazard (e.g. geological conditions and earthquakes; Mulder et al. 1994), we should take mitigation measures and be prepared where possible. For most of the land areas in Switzerland, well-established hazard maps exist (Heinimann et al. 1998; Lateltin 2002). However, subaquatic hazards are not included so far. This study emphasizes the need of including subaqueous earthquake-triggered landslide hazard also in the official hazard maps.

References

Aleotti P, Chowdhury R (1999) Landslide hazard assessment: summary review and new perspectives. Bull Eng Geol Environ 58:21–44. doi:10.1007/s100640050066

Bellugi D, Milledge DG, Dietrich WE, Perron JT, McKean J (2015) Predicting shallow landslide size and location across a natural landscape: Application of a spectral clustering search algorithm. J Geophys Res Earth Surf 120:2552–2585. doi:10.1002/2015JF003520

Bertoldi CE (1988) Computer simulation of progressive failure in soil slopes. Doctor of Philosophy thesis, Department of Civil and Mining Engineering, University of Wollongong

Bollinger D (1996) Erfassung, Darstellung und Beurteilung von Naturgefahren - Sinn und Zweck. In: Oddson B (ed) Instabile Hänge und andere risikorelevante natürliche Prozesse - Nachdiplomkurs in angewandten Erdwissenschaften. Birkhäuser, Basel, pp 55–66

Bray JD, Travasarou T (2009) Pseudostatic coefficient for use in simplified seismic slope stability evaluation. J Geotech Geoenviron Eng 135:1336–1340. doi:10.1061/(ASCE)GT.1943-5606.0000012

Chapron E, Beck C, Pourchet M, Deconinck JF (1999) 1822 earthquake-triggered homogenite in Lake Le Bourget (NW Alps). Terra Nova 11:86–92. doi:10.1046/j.1365-3121.1999.00230.x

Dan G, Sultan N, Savoye B (2007) The 1979 Nice harbour catastrophe revisited: trigger mechanism inferred from geotechnical measurements and numerical modelling. Mar Geol 245:40–64. doi:10.1016/j.margeo.2007.06.011

Dimmock P, Mackenzie B, Mills AJ (2012) Probabilistic slope stability analysis in the West Nile Delta, offshore Egypt. In: Allan P (eds) Offshore site investigation and geotechnics. Proceedings of the 7th International Offshore site Investigation and Geotechnics Conference, London, pp 535–542

Dobry R, Borcherdt RD, Crouse CB, Idriss IM, Joyner WB, Martin GR, Power MS, Rinne EE, Seed RB (2000) New site coefficients and site classification system used in recent building seismic code provisions. Earthq Spectra 16:41–67. doi:10.1193/1.1586082

European Commitee for Standardization (2004) Eurocode 8: Design of structures for earthquake resistance—Part 1: General rules, seismic actions and rules for buildings. European Committee for Standardization 1:231. Authority: The European Union per Regulation 305/2011, Directive 98/34/EC, Directive 2004/18/EC

Ewing J, Carter JA, Sutton GH, Barstow N (1992) Shallow-water sediment properties derived from high-frequency shear and interface waves. J Geophys Res Solid Earth 97:4739–4762. doi:10.1029/92jb00180

Fäh D, Giardini D, Kästli P, Deichmann N, Gisler M, Schwarz-Zanetti G, Alvarez-Rubio S, Sellami S, Edwards B, Allmann B, Bethmann F, Wössner J, Gassner-Stamm G, Fritsche S, Eberhard D (2011)

ECOS-09 Earthquake Catalogue of Switzerland Release 2011. Report and Database, Public catalogue, 17 Apr 2011, Zürich

Fedele JJ, García MH (2009) Laboratory experiments on the formation of subaqueous depositional gullies by turbidity currents. Mar Geol 258:48–59. doi:10.1016/j.margeo.2008.11.004

Field ME, Gardner JV, Prior DB (1999) Geometry and significance of stacked gullies on the northern California slope. Mar Geol 154:271–286. doi:10.1016/S0025-3227(98)00118-2

Girardclos S, Schmidt OT, Sturm M, Ariztegui D, Pugin A, Anselmetti FS (2007) The 1996 AD delta collapse and large turbidite in Lake Brienz. Mar Geol 241:137–154. doi:10.1016/j.margeo.2007.03.011

Grilli ST, Taylor ODS, Baxter CDP, Maretzki S (2009) A probabilistic approach for determining submarine landslide tsunami hazard along the upper east coast of the United States. Mar Geol 264:74–97. doi:10.1016/j.margeo.2009.02.010

Hammond CJ, Prellwitz RW, Miller SM (1991) Landslide hazard assessment using Monte Carlo simulation. In: Bell DH (ed) Landslides. Balkema, Rotterdam, pp 959–964

Heim A (1876) Bericht und Expertengutachten über die im Februar und September 1875 in Horgen am Zürichsee vorgekommenen Rutschungen. Die Eisenbahn 4:191–196

Heinimann HR, Hollenstein K, Kienholz H, Krummenacher B, Mani P (1998) Methoden zur Analyse und Bewertung von Naturgefahren. Umw Mater Nat 85:248

Henriod S, Douard R, Ullmann D, Humbel R (2016) Statistik der Bevölkerung und Haushalte (STATPOP). Bundesamt für Statistik (BFS), Bern. BFS-Nummer: be-d-00.03-13-STATPOP-v16

Hilbe M, Anselmetti FS (2014) Signatures of slope failures and river-delta collapses in a perialpine lake (Lake Lucerne, Switzerland). Sedimentology. doi:10.1111/sed.12120

Hilbe M, Anselmetti FS (2015) Mass movement-induced tsunami hazard on Perialpine Lake Lucerne (Switzerland): scenarios and numerical experiments. Pure appl Geophys 172:545–568. doi:10.1007/s00024-014-0907-7

Hoffmann G, Reicherter K (2016) Geohazards: coastal disasters. In: Harff J, Meschede M, Petersen S, Thiede J (eds) Encyclopedia of marine geosciences. Springer, Dordrecht, pp 276–283

Hunter JA, Burns RA, Good RL, Aylsworth JM, Pullan SE, Perret D, Douma M (2007) Borehole shear wave velocity measurements of Champlain Sea sediments in the Ottawa-Montreal region

ISSMGE (2004) Glossary of risk assessment terms—version 1. TC32—Technical Committee on Risk Assessment and Management, vol 66, pp 1–7

Izumi N (2004) The formation of submarine gullies by turbidity currents. J Geophys Res 109:1–13. doi:10.1029/2003JC001898

Jibson RW (2011) Methods for assessing the stability of slopes during earthquakes—a retrospective. Eng Geol 122:43–50. doi:10.1016/j.enggeo.2010.09.017

Jibson RW, Harp EL, Michael JA (2000) A method for producing digital probabilistic seismic landslide hazard maps. Eng Geol 58:271–289

Kelts K (1978) Geological and sedimentary evolution of Lakes Zurich and Zug, Switzerland. PhD thesis, No. 6146, ETH Zurich

Kelts K, Hsü KJ (1980) Resedimented facies of 1875 Horgen slumps in Lake Zurich and a process model of longitudinal transport of turbidity currents. Eclogae Geol Helv 73:271–281

Kelts K, Briegel U, Ghilardi K, Hsu K (1986) The limnogeology-ETH coring system. Swiss J Hydrol 48:104–115. doi:10.1007/BF02544119

Kramer SL (1996) Geotechnical Earthquake Engineering. Prentice-Hall, Upper Saddle River, p 653

Kremer K, Simpson G, Girardclos S (2012) Giant Lake Geneva tsunami in AD 563. Nat Geosci 5:756–757

Kremer K, Hilbe M, Simpson G, Decrouy L, Wildi W, Girardclos S (2015) Reconstructing 4000 years of mass movement and tsunami history in a deep peri-Alpine lake (Lake Geneva, France–Switzerland). Sedimentology. doi:10.1111/sed.12190

Kuen E (1999) Der Uferabbruch im Kusen. In: Küsnachter Jahrheft. Ortsgeschichtliche Kommission der Kulturellen Vereinigung Küsnacht, pp 44–50

L'Heureux J-S, Hansen L, Longva O, Eilertsen RS (2013) Landslides along Norwegian fjords: causes and hazard assessment. In: Margottini C, Canuti P, Sassa K (eds) Landslide science and practice. Springer, Berlin, pp 81–87

Lateltin OJ (2002) Landslides, land-use planning and risk management: Switzerland as a case-study. In: McInnes RG, Jakeways J (eds) Instability: planning and management. Thomas Telford, London, pp 89–96

Lee EM, Jones DKC (2014) Landslide risk assessment, 2nd edn. ICE Publishing, London

Leroueil S, Vaunat J, Picarelli L, Locat J, Lee H, Faure R (1996) Geotechnical characterisation of slope movements. In: Senneset K (ed) Landslides, 1st edn. Balkema, Rotterdam, pp 53–74

Melo C, Sharma S (2004) Seismic coefficients for pseudostatic slope analysis. Paper no. 369

Micallef A, Mountjoy JJ (2011) A topographic signature of a hydrodynamic origin for submarine gullies. Geology 39:115–118. doi:10.1130/G31475.1

Moernaut J, De Batist M (2011) Frontal emplacement and mobility of sublacustrine landslides: results from morphometric and seismostratigraphic analysis. Mar Geol 285:29–45. doi:10.1016/j.margeo.2011.05.001

Moernaut J, De Batist M, Charlet F, Heirman K, Chapron E, Pino M, Brümmer R, Urrutia R (2007) Giant earthquakes in South-Central Chile revealed by Holocene mass-wasting events in Lake Puyehue. Sed Geol 195:239–256. doi:10.1016/j.sedgeo.2006.08.005

Monecke K, Anselmetti FS, Becker A, Sturm M, Giardini D (2004) The record of historic earthquakes in lake sediments of Central Switzerland. Tectonophysics 394:21–40. doi:10.1016/j.tecto.2004.07.053

Mueller C, Mountjoy J, Power W, Lane E, Wang X (2016) Towards a spatial probabilistic submarine landslide hazard model for submarine canyons. In: Lamarche G, Mountjoy J, Bull S et al (eds) Submarine mass movements and their consequences. Springer, Cham, pp 589–597

Mulder T, Tisot JP, Cochonat P, Bourillet JF (1994) Regional assessment of mass failure events in the Baie des Anges, Mediterranean Sea. Mar Geol 122:29–45. doi:10.1016/0025-3227(94)90203-8

Nadim F, Kalsnes B, Eide A (1996) Analysis of submarine slope stability under seismic action. In: Senneset K (ed) Landslides. Balkema, Rotterdam, pp 561–565

Nipkow F (1927) Über das Verhalten der Skelette planktischer Kieselalagen im geschichteten Tifenschlamm des Zürich- und Baldeggersees. PhD thesis, No. 455, ETH Zurich

Praet N, Moernaut J, Van Daele M, Boes E, Haeussler PJ, Strupler M, Schmidt S, Loso MG, De Batist M (2016) Paleoseismic potential of sublacustrine landslide records in a high-seismicity setting (south-central Alaska). Mar Geol. doi:10.1016/j.margeo.2016.05.004

Reusch A, Moernaut J, Anselmetti FS, Strasser M (2016) Sediment mobilization deposits from episodic subsurface fluid flow—a new tool to reveal long-term earthquake records? Geology 44:243–246. doi:10.1130/G37410.1

Schnellmann M, Anselmetti FS, Giardini D, McKenzie JA, Ward SN (2002) Prehistoric earthquake history revealed by lacustrine slump deposits. Geology 30:1131–1134. doi:10.1130/0091-7613(2002)030<1131:PEHRBL>2.0.CO;2

Shillington DJ, Seeber L, Sorlien CC, Steckler MS, Kurt H, Dondurur D, Çifçi G, Imren C, Cormier MH, McHugh CMG, Gürçay S, Poyraz D, Okay S, Atgin O, Diebold JB (2012) Evidence for widespread creep on the flanks of the sea of Marmara transform basin from marine geophysical data. Geology 40:439–442. doi:10.1130/G32652.1

Smith SB, Karlin RE, Kent GM, Seitz GG, Driscoll NW (2013) Holocene subaqueous paleoseismology of lake tahoe. Bull Geol Soc Am 125:691–708. doi:10.1130/B30629.1

Strasser M, Anselmetti FS (2008) Mass-movement event stratigraphy in Lake Zurich; a record of varying seismic and environmental impacts. Beitr Geol Schweiz 95:23–41

Strasser M, Anselmetti FS, Fäh D, Giardini D, Schnellmann M (2006) Magnitudes and source areas of large prehistoric northern Alpine earthquakes revealed by slope failures in lakes. Geology 34:1005. doi:10.1130/G22784A.1

Strasser M, Stegmann S, Bussmann F, Anselmetti FS, Rick B, Kopf A (2007) Quantifying subaqueous slope stability during seismic shaking: Lake Lucerne as model for ocean margins. Mar Geol 240:77–97. doi:10.1016/j.margeo.2007.02.016

Strasser M, Hilbe M, Anselmetti FS (2011) Mapping basin-wide subaquatic slope failure susceptibility as a tool to assess regional seismic and tsunami hazards. Mar Geophys Res 32:331–347. doi:10.1007/s11001-010-9100-2

Strasser M, Monecke K, Schnellmann M, Anselmetti FS (2013) Lake sediments as natural seismographs: a compiled record of Late Quaternary earthquakes in Central Switzerland and its implication for Alpine deformation. Sedimentology 60:319–341. doi:10.1111/sed.12003

Strupler M, Hilbe M, Anselmetti FS, Strasser M (2015) Das neue Tiefenmodell des Zürichsees: Hochauflösende Darstellung der geomorphodynamischen Ereignisse im tiefen Seebecken. Swiss Bull Angew Geol 20:71–83

Strupler M, Hilbe M, Anselmetti FS, Kopf AJ, Fleischmann T, Strasser M (2017) Probabilistic stability evaluation and seismic triggering scenarios of submerged slopes in Lake Zurich (Switzerland). Geo Mar Lett 37:241–258. doi:10.1007/s00367-017-0492-8

Sultan N, Cochonat P, Canals M, Cattaneo A, Dennielou B, Haflidason H, Laberg JS, Long D, Mienert J, Trincardi F, Urgeles R, Vorren TO, Wilson C (2004) Triggering mechanisms of slope instability processes and sediment failures on continental margins: a geotechnical approach. Mar Geol 213:291–321. doi:10.1016/j.margeo.2004.10.011

Terlien MTJ (1996) Modelling spatial and temporal variations in rainfall triggered landslides: the integration of hydrologic models, slope stability models and geographic information systems for the hazard

zonation of rainfall-triggered landslides with examples from Manizal. PhD thesis, International Institute for Aerospace Survey and Earth Sciences (ITC)

Terzaghi K (1951) Mechanisms of landslides. Harvard University, Harvard

Urgeles R, Locat J, Lee HJ, Martin F (2002) The Saguenay Fjord, Quebec, Canada: integrating marine geotechnical and geophysical data for spatial seismic slope stability and hazard assessment. Mar Geol 185:319–340. doi:10.1016/S0025-3227(02)00185-8

Vessia G, Rainone ML, Signanini P (2015) Vs and NSPT measures for seismic characterization of soils. In: Lollino G, Manconi A, Guzzetti F, Culshaw M, Bobrowsky P, Luino F (eds) Engineering geology for society and territory. Springer, Cham, pp 1143–1147

Waldmann N, Anselmetti FS, Ariztegui D, Austin JA Jr, Pirouz M, Moy CM, Dunbar R (2011) Holocene mass-wasting events in Lago Fagnano, Tierra del Fuego (54°S): implications for paleoseismicity of the Magallanes-Fagnano transform fault. Basin Res 23:171–190. doi:10.1111/j.1365-2117.2010.00489.x

Wang HB, Liu GJ, Xu WY, Wang GH (2005) GIS-based landslide hazard assessment: an overview. Prog Phys Geogr 29:548–567. doi:10.1191/0309133305pp462ra

Wiemer S, Giardini D, Fäh D, Deichmann N, Sellami S (2009) Probabilistic seismic hazard assessment of Switzerland: best estimates and uncertainties. J Seismol 13:449–478. doi:10.1007/s10950-008-9138-7

Wiemer S, Danciu L, Edwards B, Marti M, Fäh D, Hiemer S, Wössner J, Cauzzi C, Kästli P, Kremer K (2016) Seismic hazard model 2015 for Switzerland, pp 1–163. doi:10.12686/a2